Nanoscale

PAPER

View Article Online
View Journal | View Issue

Cite this: *Nanoscale*, 2018, **10**, 11485

Kinetic monitoring of glutathione-induced silver nanoparticle disintegration†

Claudia Kästner, Patrick E. J. Saloga and Andreas F. Thünemann *

Received 22nd March 2018,
Accepted 7th May 2018

DOI: 10.1039/c8nr02369g

rsc.li/nanoscale

We report on etching of polyacrylic acid-stabilised silver nanoparticles in the presence of glutathione (GSH). The initial particles with a radius of 3.2 nm and consisting of ~8100 silver atoms dissolve in a two-step reaction mechanism while in parallel smaller silver particles with a radius of 0.65 nm and consisting of 60 to 70 silver atoms were formed. The kinetics of the etching of the initial particles, accompanied by formation of smaller silver particles was interpreted based on *in situ*, time-resolved small-angle X-ray scattering (SAXS) experiments.

Introduction

Today the commercial, societal, and environmental impacts of a wide range of emerging silver nanoparticle technologies is under highly controversial dispute as reviewed recently by Calderón-Jiménez *et al.*[1] The pivotal point of this debate is the release of large amounts of silver ions from silver nanoparticles, which in turn show complex chemical transformations in biological environments.[2] An intriguing work of the transformation of silver nanoparticles is a study of Glover *et al.*[3] who have shown that new silver nanoparticles can be generated spontaneously from "parent" nanoparticles and from manmade macroscopic silver objects. These findings are of general importance because nowadays the typical dietary intake of humans is estimated at 70 to 90 μg silver per day.[4] In contrast to the unintentional ingestion of silver in different chemical and physical forms, the controlled release of biologically active silver from "nanosilver" surfaces is of great interest in a multitude of antibacterial applications.[5] It should be noted that the appearance of bacterial resistance to silver nanoparticles and strategies how to overcome this issue are under debate.[6]

When considering properties of silver nanoparticles, type and amount of coating ligands are of paramount importance. Ligands enable the setting of tailor-made properties such as colloidal stability, antibacterial behaviour, silver ion release kinetics and accessibility of particles' surfaces for substrates in catalytic reactions. An example for adjusting catalytic activity *via* choice of the ligand is the application of small silver nanoparticles with different coatings in the reduction of 4-nitrophenol. Here, the activity can be tuned from 436 to 77.6 L g^{-1} s^{-1} if the ligand polyacrylic acid (PAA) is replaced by glutathione (GSH).[7]

In nanoparticle research, GSH is of great interest because it is highly biocompatible and has a strong binding affinity to metal surfaces. As a natural tripeptide GSH is the most abundant intracellular thiol with several biological functions and is the major antioxidant in liver.[8] Probably because of its low molar mass of 307 g mol^{-1}, GSH is capable of effectively stabilising small silver nanoparticles down to radii of about 0.5 to 1 nm.[9] These so-called silver clusters are not only of fundamental scientific interest, but are also useful for many applications[10] such as fluorescent labels in bioimaging.[9] But apart from its undeniable advantages, GSH has some contradictory properties: under ambient conditions, a spontaneous formation of silver nanoparticles was observed when GSH is in contact with silver nitrate solutions. Furthermore, GSH was also found to induce the disintegration of silver nanoparticles.[11] Unfortunately, the role of GSH in particle formation, stabilisation, and disintegration is presently unclear and, therefore, a subject of current research.

In this context, it is the aim of our study to understand the fate of silver nanoparticles in the presence of GSH. We utilised well defined spherical silver nanoparticles for this purpose, which were employed as performance test material in a recent interlaboratory comparison on nanoparticles size distribution quantification.[12] We incubated these particles with GSH in aqueous environment and monitored changes of particles characteristics with SAXS. Within this investigation, we provide a detailed insight into the disintegration of silver nanoparticles and formation of new smaller particles.

Results and discussion

For the synthesis of the initial silver nanoparticles, stabilised by PAA, we used a variation of the widely used polyol syn-

Federal Institute for Materials Research and Testing (BAM), Unter den Eichen 87, 12205 Berlin, Germany. E-mail: andreas.thuenemann@bam.de

†Electronic supplementary information (ESI) available: TEM images and long-time SAXS data. See DOI: 10.1039/c8nr02369g

thesis[13] as described in the Experimental section. After adding GSH to the silver nanoparticles in a molar ratio of 1 to 5 (silver atoms to GSH molecules), the mixture was incubated at a temperature of 21 °C. According to literature,[11] we expected that GSH continuously etches the silver nanoparticles, resulting in a decreasing radius and finally in their dissolution. SAXS was employed to follow the etching process over a period of 240 h. Radii distributions of the particles and their volume concentrations were determined from SAXS data with the help of a Monte Carlo method.[14]

A comprehensive overview on the particle population as a function of incubation time is provided in Fig. 1. Therein, the initial radii distribution is monomodal while, surprisingly, the radii distribution of the incubated particles is bimodal. Radii and volume fractions of the larger particles continuously decreased while a population of small particles emerged. Examples of two typical scattering curves – one measured directly after addition of GSH and a second curve measured after 66 h incubation time – are displayed in Fig. 2. The distributions are slightly asymmetric around their maxima, with tails decaying more slowly towards larger radii. Therefore, symmetric functions such as a Gaussian profile cannot be considered for their description, but a lognormal function describes the distribution sufficiently well as confirmed earlier for the pristine particles.[12] When employing the lognormal distribution for interpretation, we found a volume-weighted mean particle radius of R = (3.22 ± 0.02) nm and a width of σ = (0.56 ± 02) nm for the pristine particles. This is in accordance with the results from our recent inter-laboratory comparison.[12] These particles consist of *ca.* 8100 silver atoms if a single silver atom requires a space of 0.0171 nm^3 as in bulk silver. In contrast, after 66 h of incubation we determined a population of particles (p_{large}) with a mean radius of R = (2.51 ± 0.01) nm and a width of σ = (0.43 ± 0.01) nm and a second population of smaller particles (p_{small}) with a mean radius of R = (0.65 ± 0.02) nm and a width of σ = (0.18 ± 0.01) nm. The corresponding numbers of silver atoms per particle are *ca.* 4000 and 60 to 70, respectively. Both particle populations p_{small} and p_{large} have a relative volume fraction of 50% as can be seen from the CDF and are well separated with a minimum in the PDF at about 1.3 nm. Attempts in using TEM to reveal the particle structure after incubation with GSH confirm that the particles are in the size range derived from SAXS. Unfortunately, only the particle population p_{large} is clearly visible in the micrographs, while the population p_{small} is below the resolution of the TEM instrument (see ESI, Fig. S1†). To elucidate whether the small particle population is significant, we performed SAXS measurements with extended measurement times of 24 h. This provides higher quality data statistics to confirm the bimodal size distribution (see ESI, Fig. S2†). Indeed, we found no significant difference in the resultant bimodal size distributions when short and long time SAXS measurements were used for data evaluation.

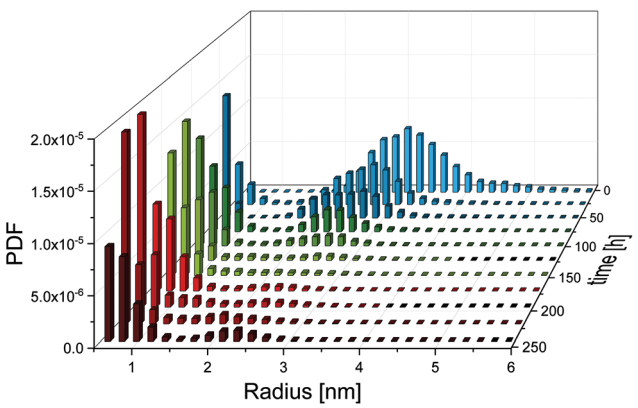

Fig. 1 Glutathione-induced changes of the radii of silver particles. Presented are volume weighted partial differential functions (PDF) of the radii determined at 1, 24, 48, 72, 96, 120, 144, 168, 192, 216, and 240 h after addition of glutathione.

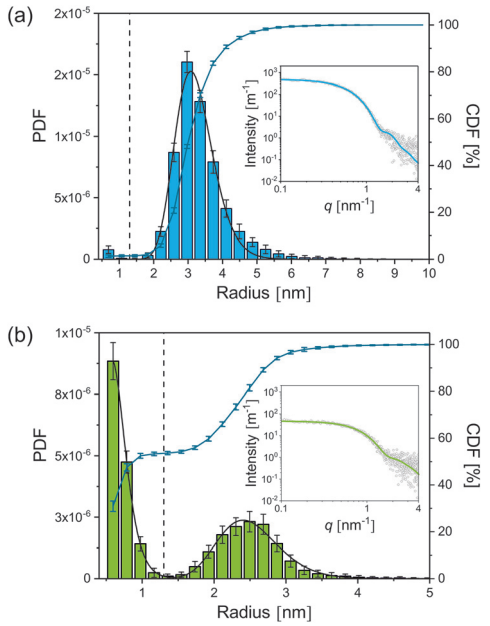

Fig. 2 Volume-weighted size distributions of silver nanoparticles determined at times of t = 0 and 66 h after adding GSH (a and b, respectively). Displayed are partial differential functions (PDF, histograms), best fit curves using lognormal functions (solid black lines) and cumulative distribution functions (CDF, solid blue lines). PDFs are given as volume fraction, CDFs as volume fraction in percentage. Vertical dashed lines at 1.3 nm show the boundary between the two nanoparticle populations p_{small} and p_{large}. The insets show the SAXS data along with their best curve fits (symbols and solid lines, respectively).

Based on the SAXS data, we can draw the hypothesis that incubation with GSH leads to the formation of "new", very small silver particles at the expense of the "old", larger particles. Two different pathways are conceivable: (i) the larger particles are "etched" and simply decrease in radius, or (ii) two parallel processes take place – the etching of the larger particles and coincidently the formation of new small particles. To reveal the reaction pathway, detailed evaluations of time-dependent changes of particle radii, particle mass concen-

trations, particle surface areas and particle numbers are provided in the following.

As a first parameter changes of the radii of both particle populations in dependence of incubation time were evaluated (Fig. 3). The p_{small} were first observed at an incubation time of three hours. Their median radius R_{small} = (0.66 ± 0.02) nm was constant over time and showed a size distribution of moderate width (Fig. 3a). In contrast, the radius of p_{large} decreased continuously according to a power law (Fig. 3b):

$$R_{large} = (3.1 \pm 0.1\ \text{nm}) t^{-(0.063 \pm 0.003)}$$

While a decrease of R_{large} was expected, the finding of a constant value of R_{small} was surprising. Typically, a coalescence of particles or an Ostwald ripening occurs after nucleation of particles,[15,16] whereas in the present study particle growth stopped at a very early stage. The reason for this is unclear, but we speculate that these newly formed smaller nanoparticles are energetically preferred, since GSH seems to efficiently stabilise silver nanoparticles of this selected size. Our finding is consistent with results of Desireddy *et al.*[17] who investigated highly stable thiolate-protected silver nanoclusters. We assume that also silver glutathione clusters containing only a few silver atoms (sub-nanometer particles) could be present during our etching experiment. In literature, clusters of 11 silver atoms are reported by Baksi *et al.*[18] and clusters of 9 and 16 silver atoms are described by Yuan *et al.*[19] Observation of sub-nanometer particles containing only a few silver atoms is below the size detection limit of SAXS. Therefore, these sub-nanometer particles remain "invisible" for SAXS and are not included in the resulting size distribution.

For investigation of the reaction pathway, determination of changes in particle concentration of p_{large} and p_{small} is inevitable. Based on that, conclusions can also be drawn about the concentration of the non-detectable sub-nanometer particles. Particle concentrations were determined from SAXS data according to the procedure evaluated in our recent interlaboratory comparison.[12] Values for p_{small}, p_{large} and the total particle concentration p_{small} + p_{large} are shown in Fig. 4. The concentration of p_{small} increased continuously while that of p_{large} decreased. For p_{large}, the concentration is reduced from an initial value of *ca.* 0.7 g L^{-1} to a minimum concentration of 0.04 g L^{-1} at 100–150 h. This corresponds to a mass shrinkage of p_{large} by 94%. In contrast, the concentration of p_{small} reaches a limit in the range of 0.4 to 0.5 g L^{-1} at times longer than 150 h. It should be noted that a small amount of p_{large} could still be found after an incubation period of 240 h, indicating that the particle population p_{large} was not completely dissolved. In addition to ambient conditions, the experiment was also carried out in absence of oxygen by using argon gas as protecting atmosphere, which resulted in no significantly different outcome. Therefore, we exclude that the presence of oxygen has a substantial influence on changes of the radii distributions. Instead, GSH seems to predominately promote the transformation process of the particles size distribution. This finding is in accordance with a recent study of Baksi *et al.*[20] who investigated the reactivity of GSH stabilised silver clusters $Ag_{11}(GSH)_7$ and $Ag_{32}(GSH)_{32}$. They show that oxygen has no major influence on the degradation of these clusters by an excess of GSH. Conclusively, the initial concentration of p_{large} was 0.7 g L^{-1} and the final concentration of p_{small} is around 0.5 g L^{-1}, whereas the final concentration of p_{large} is 0.04 g L^{-1}. Therefore, we assume that about 0.2 g L^{-1} of silver was present in form of "invisible" sub-nanometer particles.

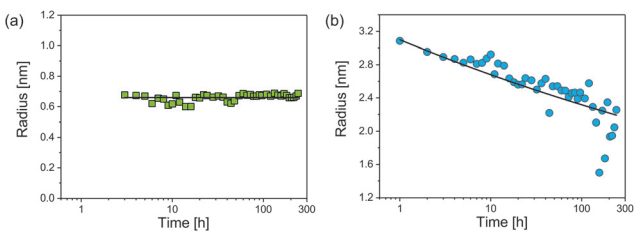

Fig. 3 Radii (median values) of the two particle populations p_{small} (a) and p_{large} (b). Particles p_{small} were first detected at an incubation time of 3 h and display constant radii of R_{small} = 0.66 ± 0.01 nm (solid black line in (a)). Radii of particles p_{large} display a power law decay according to $R_{large} = R_0\ t^{-p}$ with R_0 = 3.1 nm and p = 0.063 ± 0.003 (solid black curve in (b)).

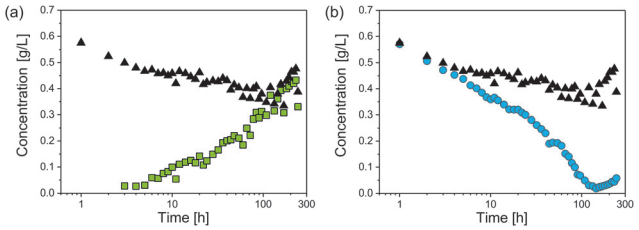

Fig. 4 Mass concentration of the two particle populations p_{small} (green squares in (a)) and p_{large} (blue circles in (b)) as a function of incubation time. The total mass concentration c_{total} = c_{small} + c_{large} is given in figures (a) and (b) for comparison (black triangles).

An appropriate assumption is that the etching kinetics of the particles p_{large} are strongly influenced by particles' surface area exposed to GSH molecules. Therefore, the specific surface area of the particles per volume ($S_{V,small}$ and $S_{V,large}$) was determined as a function of time from the volume fraction of the particles (φ_{small} and φ_{large}) and the particles' median radius ($R_{V,smll}$ and $R_{V,large}$) as

$$S_{V,small} = \frac{3\varphi_{small}}{R_{V,small}} \text{ and } S_{V,large} = \frac{3\varphi_{large}}{R_{V,large}} \quad (1)$$

We found that $S_{V,small}$ of p_{small} increases continuously with time while $S_{V,large}$ of p_{large} can be divided into three periods that change approximately linearly with time as shown in Fig. 5. $S_{V,large}$ decreases fast within period 1, slowly in period 2 and stays approximately constant in period 3 (Fig. 5b). Linear functions were fitted for quantification of the three periods,

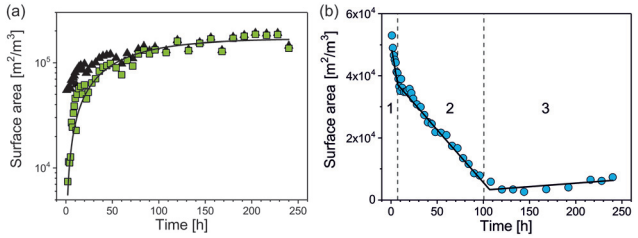

Fig. 5 Changes of the surface area of particles p_{small} (squares in (a)) and p_{large} (spheres in (b)) as a function of time after addition of GSH. The total surface area of all particles is provided in (a) for comparison (black triangles). Solid black lines in (a) and (b) present best curve fits. The change of the surface area of p_{large} is fitted with a piecewise linear function of different slopes in region 1, 2 and 3. The increase of the surface area of p_{small} is fitted by an exponential function.

each with a reaction constant k_i and $S_{V,i}(0)$ – the specific surface area extrapolated to $t = 0$ – with $i = 1, 2, 3$:

$$S_{V,large,i}(t) = S_{V,large,i}(0) - k_i \cdot t \quad (2)$$

Eqn (2) corresponds to reaction kinetics of zero order with respect to the specific particle surface area. Such a linear decrease of $S_{V,large}$ with time is in line with our expectations regarding the etching process. Utilising eqn (2) revealed that the initial specific surface area of p_{large} was $S_{V,large,1}(t = 0) = (53\,000 \pm 1000)$ m^2 m^{-3}. The $S_{V,large,1}(t)$ decreased with a rate constant of $k_1 = (1850 \pm 180)$ m^2 m^{-3} h^{-1} to $S_{V,large,1}(t_1) = (39\,900 \pm 3400)$ m^2 m^{-3} at $t_1 = (7.1 \pm 0.6)$ h (Fig. 5b). This corresponds to a surface area reduction of 25% within period 1. $S_{V,large}$ was further reduced in period 2 with a lower rate constant of $k_2 = (350 \pm 10)$ m^2 m^{-3} h^{-1} down to $S_{V,large,2}(t_2) = (5400 \pm 2100)$ m^2 m^{-3} at $t_2 = (100.5 \pm 1.7)$ h. Therefore, about 10% of the initial surface area remains at the end of period 2. This value is almost constant in period 3 with a slight trend of increase with a rate constant of $k_3 = (-23 \pm 9)$ m^2 m^{-3} h^{-1}. All fitting parameters are summarised in Table 1. For interpretation of the different etching kinetics in period 1 and 2, we assumed that polyacrylic acid was firstly exchanged by GSH in period 1 because binding of the SH group of GSH to silver is much stronger than that of the carboxylic acid groups of polyacrylic acid.[21] It is reasonable that GSH acts as etching agent but also passivates the silver nanoparticle surface. An overlay of passivation and etching provides a possible explanation why the etching process was significantly slower in period 2 than in 1. Since p_{large} did not disappear completely at the end of the measurement time, we conclude that a more complex reaction scenario than simple etching is present.

Table 1 Best fit parameters of the piecewise linear function applied for approximation of the change of the specific surface area $S_{v,large}$ of particles p_{large}

Region	Time interval [h]	$S_v(0)$ [m^2 m^{-3}]	k [m^2 m^{-3} h^{-1}]
1	$0 < t < t_1 = 7.1 \pm 0.6$	$53\,000 \pm 1000$	1850 ± 180
2	$t_1 < t < t_2 = 100.5 \pm 1.7$	$40\,600 \pm 500$	350 ± 10
3	$t_2 < t < t_3 = 240$	800 ± 400	-23 ± 9

It has been reported in literature that silver nanoparticles can be nucleated from silver-GSH salts, which are formed by combination of silver ions and GSH in aqueous solution.[11] Similarly, this model can be adapted for the generation of GSH-stabilised silver particles through etching of p_{large} and subsequent silver nanoparticle formation of p_{small}. The change of the specific surface area of p_{small} as a function of time can be quantified with the exponential function

$$S_{V,small}(t) = S_{V,small}(\infty) \cdot (1 - e^{-k \cdot t}) \quad (3)$$

where $S_{V,small}(\infty)$ is the specific surface area extrapolated to infinite times and k is the rate constant of the formation of p_{small}. Data and curve fit of eqn (3) with $S_{V,small}(\infty) = (169 \pm 6) \times 10^3$ m^2 m^{-3} and $k = (0.0166 \pm 0.0016)$ h^{-1} are shown in Fig. 5a. Eqn (3) corresponds mathematically to an equation of first order reaction kinetics for formation of the surface area of p_{small}.[22] The observed increase of the specific surface area can be explained mechanistically in analogy to silver nanoparticle formation from aqueous solutions of GSH and silver nitrate reported in literature.[11] For consistency check, it is of interest to calculate the theoretically possible maximum value of the particle surface as

$$S_{V,theory} = \frac{3\varphi_{tot}}{R_{small}} = \frac{3c_{Ag}}{R_{small} \cdot \rho_{Ag}}, \quad (4)$$

where an R_{small} of 0.66 nm is the radius of p_{small}, φ_{tot} is the total volume fraction of all pristine silver nanoparticles, $c_{Ag} = 0.7$ g L^{-1} is the total silver concentration and $\rho_{Ag} = 10.49$ g cm^{-3} is the density of silver. Using these values, we calculated $S_{V,theory} = 3 \times 10^5$ m^2 m^{-3}. We conclude that about 56% of the pristine silver nanoparticles are converted into small particles, 1% of the silver is deposited in particles p_{large} (with $R_{large} = 2.2$ nm) and the rest of silver is present in form of subnanometer silver particles. Attempts of using higher molar ratios than 5 : 1 of GSH to silver with the aim to completely dissolve p_{large}, led to formation of a black precipitate.

Finally, we consider the number of particles p_{small} and the total number of particles p_{small} + p_{large} (Fig. 6). After 7 h the

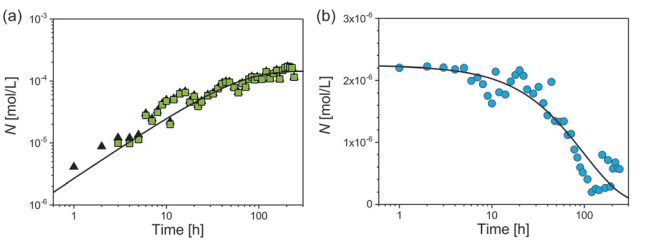

Fig. 6 Changes of the number of particles p_{small} (squares in (a)) and p_{large} (spheres in (b)) as a function of time after addition of GSH. The total number of all particles is provided in (a) for comparison (black triangles). The black solid line in (a) is the best curve fit of first order kinetics that describes the increase of the number of p_{small}. The solid black line in (b) corresponds to the best curve fit of an exponential decay function with a lag time.

number of p_{small} was closely identical to the total number of particles. At this stage of reaction and later the contribution of p_{small} was determinant for the total particle number. The increase of the number of p_{small} can be described by an exponential growth function as

$$N_{small} = \Delta N_{small}(1 - \exp[-k_{small}t]), \quad (5)$$

with $\Delta N_{small} = (1.45 \pm 0.07) \times 10^{-4}$ mol L^{-1}, which corresponds to N_{small} at infinite time, and $k_{small} = (0.0186 \pm 0.0023)$ h^{-1}. In analogy, the decrease of the number of p_{large} is represented by

$$N_{large} = \Delta N_{large} \exp[-k_{large}(t - t_0)], \quad (6)$$

with $\Delta N_{large} = -2.2 \times 10^{-6}$ mol L^{-1} (N_{large} at infinite time), $k_{large} = (0.0102 \pm 0.004)$ h^{-1} and $t_0 = (68 \pm 6)$ h. The t_0 indicates the delay time necessary for complete dissolution – not only etching – of a significant number of p_{large}.

From combination of both processes for p_{large} and p_{small} we conclude that $\Delta N_{small}/\Delta N_{large} = -66$, which means that for each disappearing particle p_{large} 66 new particles of p_{small} are formed. The ratio of the reaction constants k_{small}/k_{large} shows that the formation of p_{small} is significantly faster than the reduction of p_{large}. The k-values can be utilised to calculate the time τ_i required to form/dissolve 50% of the final number of particles (eqn (7)).

$$\tau_i = \ln(2)k_i^{-1} \quad (7)$$

For the formation of p_{small} this results in $\tau_{small} = (37 \pm 4)$ h. Similarly, we calculated the time τ_{large} required to dissolve 50% of the initial number of particles p_{large}, which gives $\tau_{large} = (136 \pm 9)$ h.

By combining all data derived above, we make a hypothesis for the mechanism of the observed particle transformation as sketched in Fig. 7. Therein, the transformation of p_{large} to p_{small} is assumed to be mediated by complexes of Ag and GSH. These sub-nanometer particles may be present in form of GSH stabilised Ag clusters, which contain only a few number of Ag atoms. A direct transformation of p_{large} to p_{small} must be considered as extremely unlikely because the total number of the particles did not stay constant. Therefore, we conclude that the reaction pathway (ii), consisting of two parallel processes – dissolution and formation of p_{large} and p_{small}, respectively – corresponds to the most likely reaction mechanism.

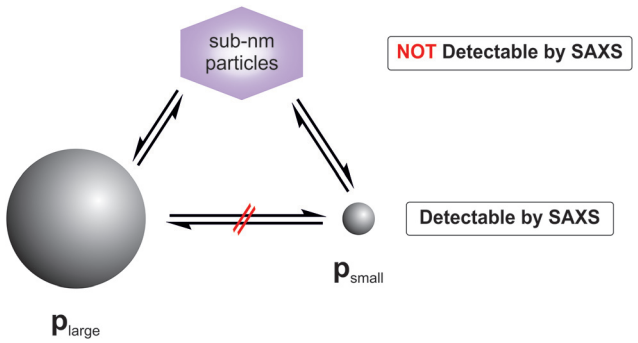

Fig. 7 Sketch of the mechanism of particle size transformation from p_{large} to p_{small} is assumed to be mediated by a complex of Ag and GSH. A direct transformation of p_{large} to p_{small} can be excluded. Particle populations of p_{large} and p_{small} can be detected with SAXS while the sub-nanometer silver particles cannot be detected.

Conclusions

The etching process of polyacrylic acid-stabilised silver nanoparticles with concurrent formation of new smaller silver nanoparticles was characterised with the help of SAXS measurements. The etching process follows zero order kinetics and can be divided in three periods: a fast etching in period one which is based on the exchange of PAA with GSH, a slow etching in period two where passivation through GSH hinders etching, and a steady-state situation in period three. In parallel, the formation of very small nanoparticles is observed which follows first order kinetics.

Experimental

Materials

All chemicals were used as received without further purification. Silver nitrate was purchased from AppliChem, polyacrylic acid (PAA) with a molar mass of M_w = 1800 g mol^{-1} (catalog number 323667-250 g) from Sigma-Aldrich, and ethylene glycol, glutathione (reduced) and sodium hydroxide from Merck. For purification, Milli-Q grade water (18.2 MΩ at 25 °C) was used.

Synthesis and etching

Silver nanoparticles were produced according to an earlier described procedure.[23] Briefly, solutions of silver nitrate (833 μL, 0.19 M) and PAA (4.167 mL, 0.03 M) in ethylene glycol were mixed and heated to 200 °C for 15 min. The resulting particles were purified by threefold addition of 11.4 mL of water followed by sedimentation. An aqueous sodium hydroxide solution (1 w/v %) was added dropwise for redispersion.

The glutathione-induced etching process was studied in an aqueous solution containing 0.7 g L^{-1} silver nanoparticles, 10 g L^{-1} glutathione and 0.25 w/v % sodium hydroxide. This corresponds to a molar ratio of 5 glutathione molecules per silver atom.

SAXS measurements

SAXS measurements were performed in a flow through capillary with a Kratky-type instrument (SAXSess from Anton Paar, Austria) at 21 ± 1 °C. Samples analysed with SAXS were used as prepared and measured for 20 minutes (120 measurement frames averaged over 10 s) The measured intensity was converted to absolute scale according to Orthaber *et al.*[24] The scattering vector q depends on the wavelength λ of the radiation (λ = 0.154 nm): $q = 4\pi/\lambda \sin\theta$. Deconvolution (slit length desmearing) of the SAXS curves was performed with the

SAXS-Quant software (Anton Paar, Austria). Curve fitting was conducted with the software McSAS (version 1.0.1).[14] Since the scattering intensity was measured on an absolute scale the volume fraction of the particles was determined in addition to the particles' volume weighted radii distribution when applying McSAS. The yields were calculated as the ratio of the experimentally determined volume fraction to the maximal possible volume fraction. The latter is calculated from the mass of silver which forms if all silver ions would have been reduced. Further, we assumed that the density of the silver particles is the same as silver in bulk form (10.49 g cm^{-3}).

(HR)TEM-imaging

(HR)TEM images were obtained from a FEI Tecnai TF 20 X-TWIN transmission electron microscope operating at an acceleration voltage of 200 kV.

Conflicts of interest

There are no conflicts to declare.

Acknowledgements

We greatly thank M. Gajewska for the TEM pictures.

References

1 B. Calderón-Jiménez, M. E. Johnson, A. R. Montoro Bustos, K. E. Murphy, M. R. Winchester and J. R. Vega Baudrit, *Front. Chem.*, 2017, **5**, 1–26.
2 J. Liu, Z. Wang, F. D. Liu, A. B. Kane and R. H. Hurt, *ACS Nano*, 2012, **6**, 9887–9899.
3 R. D. Glover, J. M. Miller and J. E. Hutchison, *ACS Nano*, 2011, **5**, 8950–8957.
4 S. W. P. Wijnhoven, W. J. G. M. Peijnenburg, C. A. Herberts, W. I. Hagens, A. G. Oomen, E. H. W. Heugens, B. Roszek, J. Bisschops, I. Gosens, D. Van De Meent, S. Dekkers, W. H. De Jong, M. van Zijverden, A. J. A. M. Sips and R. E. Geertsma, *Nanotoxicology*, 2009, **3**, 109–138.
5 J. Liu, D. A. Sonshine, S. Shervani and R. H. Hurt, *ACS Nano*, 2010, **4**, 6903–6913.
6 A. Panáček, L. Kvítek, M. Smékalová, R. Večeřová, M. Kolář, M. Röderová, F. Dyčka, M. Šebela, R. Prucek, O. Tomanec and R. Zbořil, *Nat. Nanotechnol.*, 2018, **13**, 65–71.
7 C. Kästner and A. F. Thünemann, *Langmuir*, 2016, **32**, 7383–7391.
8 Y. Chen, Y. Yang, M. L. Miller, D. Shen, H. G. Shertzer, K. F. Stringer, B. Wang, S. N. Schneider, D. W. Nebert and T. P. Dalton, *Hepatology*, 2007, **45**, 1118–1128.
9 X. Le Guével, C. Spies, N. Daum, G. Jung and M. Schneider, *Nano Res.*, 2012, **5**, 379–387.
10 A. Desireddy, B. E. Conn, J. Guo, B. Yoon, R. N. Barnett, B. M. Monahan, K. Kirschbaum, W. P. Griffith, R. L. Whetten, U. Landman and T. P. Bigioni, *Nature*, 2013, **501**, 399–402.
11 K. Siriwardana, N. Suwandaratne, G. S. Perera, W. E. Collier, F. Perez and D. Zhang, *J. Phys. Chem. C*, 2015, **119**, 20975–20984.
12 B. R. Pauw, C. Kästner and A. F. Thünemann, *J. Appl. Crystallogr.*, 2017, **50**, 1280–1288.
13 Y. Hu, J. Ge, D. Lim, T. Zhang and Y. Yin, *J. Solid State Chem.*, 2008, **181**, 1524–1529.
14 I. Bressler, B. R. Pauw and A. F. Thünemann, *J. Appl. Crystallogr.*, 2015, **48**, 962–969.
15 J. Polte, X. Tuaev, M. Wuithschick, A. Fischer, A. F. Thuenemann, K. Rademann, R. Kraehnert and F. Emmerling, *ACS Nano*, 2012, **6**, 5791–5802.
16 T. R. Bartlett, S. V. Sokolov, B. J. Plowman, N. P. Young and R. G. Compton, *Nanoscale*, 2016, **8**, 16177–16181.
17 A. Desireddy, S. Kumar, J. S. Guo, M. D. Bolan, W. P. Griffith and T. P. Bigioni, *Nanoscale*, 2013, **5**, 2036–2044.
18 A. Baksi, M. S. Bootharaju, X. Chen, H. Häkkinen and T. Pradeep, *J. Phys. Chem. C*, 2014, **118**, 21722–21729.
19 X. Yuan, M. I. Setyawati, A. S. Tan, C. N. Ong, D. T. Leong and J. Xie, *NPG Asia Mater.*, 2013, **5**, e39.
20 A. Baksi, M. S. Bootharaju, P. K. Chhotaray, P. Chakraborty, B. Mondal, S. Bhat, R. Gardas and T. Pradeep, *J. Phys. Chem. C*, 2017, **121**, 26483–26492.
21 R. A. Sperling and W. J. Parak, *Philos. Trans. R. Soc., A*, 2010, **368**, 1333.
22 S. Özkar and R. G. Finke, *J. Phys. Chem. C*, 2017, **121**, 27643–27654.
23 P. E. J. Saloga, C. Kästner and A. F. Thünemann, *Langmuir*, 2018, **34**, 147–153.
24 D. Orthaber, A. Bergmann and O. Glatter, *J. Appl. Crystallogr.*, 2000, **33**, 218–225.

